Analysis of Multipactor RF Breakdown Thresholds in Elliptical Waveguides

Ali Frotanpour, *Student Member, IEEE*, Gholamreza Dadashzadeh, *Member, IEEE*, Mahmoud Shahabadi, and Benito Gimeno, *Member, IEEE*

***Abstract*—A multipactor breakdown analysis is presented for the fundamental mode of an elliptical waveguide. A 2-D geometry of the waveguide is considered, and the numerical method of Monte Carlo based on the effective-electron approach is used. Multipactor breakdown threshold prediction is performed using the enhanced counter function. The radio-frequency (RF) breakdown threshold is obtained as a function of the frequency–gap product for different values of the ellipse eccentricity. The results indicate that decreasing the ellipse eccentricity increases the RF breakdown threshold. The results are compared with those for circular and parallel-plate waveguides.**

***Index Terms*—Effective electron, elliptical waveguide, multipactor, radio-frequency (RF) breakdown threshold.**

I. Introduction

THE MULTIPACTOR phenomenon is a critical issue that can occur in space high-power radio-frequency (RF) components, high-power microwave tubes such as klystrons and cyclotrons, and particle accelerators. In a vacuum, free electrons accelerate inside a waveguide under its RF electromagnetic field and collide with the waveguide wall, and secondary electrons can be emitted from the wall. Repeated emissions in a resonant manner cause exponential growth of electrons and result in RF breakdown [1]–[10]. Multipactor breakdown increases noise power and degrades return loss, which decreases the signal-to-noise ratio [2], [10]. In addition, the phenomenon might cause waveguide heating and detuning of microwave components such as filters [2].

Multipactor breakdown has been modeled during recent years for various waveguide geometries [2]–[18]. Many researchers have analyzed and simulated multipactor phenomena on various geometries, including the following: 1) parallel plates with a limited length and/or a waveguide iris [2], [3]; 2) a rectangular waveguide [4]–[9]; 3) a coaxial line [10]–[14]; 4) a circular waveguide [15]; 5) a hollow waveguide with a wedge-shaped cross section [16]; 6) a shielded microstrip line [17]; and 7) a dielectric-loaded parallel-plate waveguide [18]. In these studies, multiple electron trajectories are predicted using the Monte Carlo method to simulate a multipactor. Recently, the basic fundamentals of the multipactor theory have been investigated, such as the analysis of the electromagnetic radiation generated by a multipactor discharge [19], the phase stability in a two-sided multipactor [20], the nonstationary statistical theory for a multipactor [21], and the prevention of multipactor discharge using a uniaxial metamaterial [22].

On the other hand, an elliptical waveguide plays an important role in RF devices such as dual-mode filters [23]–[25] and high-power microwave sources [26], [27], where high-power RF signals potentially in a vacuum may result in multipactor breakdown. Elliptical waveguide modes have been thoroughly analyzed in recent years [28]–[30].

To the knowledge of the authors, multipactor breakdown in an elliptical waveguide has not been deeply studied in the technical literature. In this paper, the multipactor in an elliptical waveguide is analyzed, and its RF breakdown threshold is numerically obtained. First, the electromagnetic field of the fundamental elliptical mode TE_{c11} is presented, and then, the electron motion equation in the elliptical coordinate system is obtained and described. To simulate a multipactor, we use the effective-electron approach, where the electron motion equation is solved numerically using the velocity Verlet algorithm for the fundamental mode of the elliptical waveguide. After an impact, a secondary emission yield (SEY) model determines the emitted electron weightings. Finally, to predict the RF breakdown threshold, the enhanced counter function is applied. The RF breakdown thresholds are provided for four different ellipse eccentricities. They are then compared with circular and parallel-plate waveguide thresholds.

II. Theory and Model Description

In the simulation, each effective electron accelerates under an applied electromagnetic field and moves within the waveguide until it impacts to the waveguide wall. The emitted secondary effective-electron weight is determined by the SEY coefficient, considering the incident effective-electron kinetic energy, its impact angle, and the waveguide material. It is then launched from the impact point [10], [35], and the process continues until a threshold number of electron impacts have been reached.

Manuscript received August 24, 2010; revised November 1, 2010 and November 30, 2010; accepted November 30, 2010. Date of publication December 30, 2010; date of current version February 24, 2011. This work was supported in part by the Electrical and Electronics Department, Shahed University, Tehran, Iran. The review of this paper was arranged by Editor W. L. Menninger.

A. Frotanpour and G. Dadashzadeh are with the Department of Electrical Engineering, Shahed University, Tehran 33191 18651, Iran (e-mail: frotanpour@shahed.ac.ir; gdadashzadeh@shahed.ac.ir).

M. Shahabadi is with the School of Electrical and Computer Engineering, Faculty of Engineering, University of Tehran, Tehran 14399 55471, Iran (e-mail: shahabad@ut.ac.ir).

B. Gimeno is with the Departamento de Física Aplicada, Instituto de Ciencia de los Materiales, Universidad de Valencia, 46100 Valencia, Spain (e-mail: benito.gimeno@uv.es).

Color versions of one or more of the figures in this paper are available online at http://ieeexplore.ieee.org.

Digital Object Identifier 10.1109/TED.2010.2097600

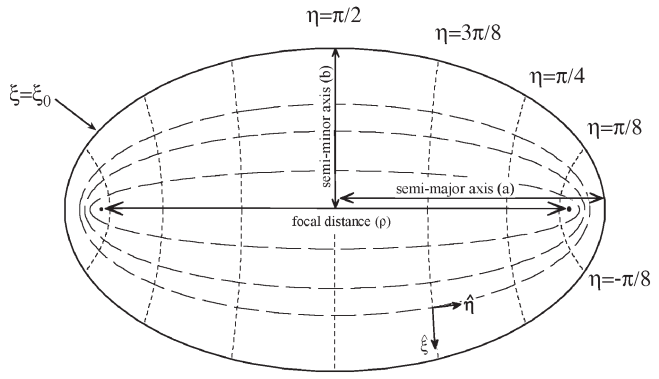

Fig. 1. Planar elliptical coordinate system. The semimajor axis length is a, the semiminor axis length is b, and the focal distance is ρ.

A. Electromagnetic Fields

The planar elliptical coordinate system is described in terms of radial (ξ) and angular (η) coordinates, as shown in Fig. 1. The electromagnetic fields of an elliptical waveguide can be obtained in this coordinate system by solving the wave equation using the method of variable separation in an elliptical coordinate system. It leads to the Mathieu and modified Mathieu functions for angular and radial components, respectively [28]. Using a series of trigonometric and hyperbolic functions, Blanch gives closed-form relations for the Mathieu and modified Mathieu functions, respectively [31]. Therefore, for the fundamental TE_{c11} mode, the magnetic field is given by

$$H_z = Ac_{e1}(q_{11}, \eta)C_{e1}(q_{11}, \xi) \tag{1}$$

where A is the normalization constant; $c_{e1}(q_{11}, \eta)$ and $C_{e1}(q_{11}, \xi)$ are the even modes of the Mathieu and modified Mathieu functions, respectively; and q_{11} is the parameter related to the cutoff wavelength λ_c for the fundamental mode, as follows:

$$\lambda_c/a = \frac{\pi e}{\sqrt{q_{11}}}. \tag{2}$$

This cutoff wavelength has been obtained using a curve-fitting method [30], in which it is demonstrated that the cutoff wavelength can be determined as a function of eccentricity by

$$\lambda_c/a = 3.41257911 - 0.06960165e^2 - 0.010811e^4 - 0.001551e^6 - 0.000196e^8 \tag{3}$$

where a is the length of the semimajor axis, and e is the ellipse eccentricity, as shown in Fig. 1.

B. Electron Dynamics

The electron motion equation for each effective electron is provided by the Lorenz force, i.e.,

$$\vec{a} = -e(\vec{E} + \vec{v} \times \vec{B})/m \tag{4}$$

where $\vec{a}$ is the acceleration vector; $\vec{v}$ is the effective-electron velocity; $\vec{E}$ is the total electric field; $\vec{B}$ is the total magnetic field; and $-e$ and m are the charge and electron mass, respectively. After some manipulations, we obtain the following equations expressed in elliptical coordinates for the 2-D motion of the effective electrons:

$$\ddot{\xi} = -\frac{e}{\rho\, m\sqrt{U}}\left[E_\xi(\xi,\eta,t) + \rho\dot{\eta}\sqrt{U}B_z(\xi,\eta,t)\right] - \left[(\dot{\xi}^2 - \dot{\eta}^2)\sinh(2\xi)/2 + \dot{\xi}\dot{\eta}\,\sin(2\eta)\right]/U \tag{5}$$

$$\ddot{\eta} = -\frac{e}{\rho\, m\sqrt{U}}\left[E_\eta(\xi,\eta,t) + \rho\dot{\xi}\sqrt{U}B_z(\xi,\eta,t)\right] - \left[(\dot{\eta}^2 - \dot{\xi}^2)\sin(2\eta)/2 + \dot{\xi}\dot{\eta}\,\sinh(2\xi)\right]/U \tag{6}$$

where

$$U = \sinh^2(\xi) + \sin^2(\eta).$$

In addition, ρ is the focal distance, $\dot{\xi}$ and $\dot{\eta}$ are the first-order time derivatives of the effective-electron position, and $\ddot{\xi}$ and $\ddot{\eta}$ are the second-order time derivatives of the effective-electron position.

Equation (5) represents the electron motion in the radial direction, which is the direction that potentially results in a wall impact. Equation (6) represents the motion in the azimuthal direction.

C. Algorithms and Models

A number of N effective electrons are initially launched from arbitrary positions inside the waveguide with randomly chosen initial velocities [10]. The phase of the RF field initially seen by each effective electron is evenly distributed from 0 to 2π. The electron trajectories are computed by solving the nonlinear system of (5) and (6) numerically, using the velocity Verlet algorithm with 200 time steps per RF period [32].

Each effective-electron trajectory is tracked until the effective electron reaches the waveguide wall, which is defined in elliptical coordinates as $\xi = \xi_0$, as shown in Fig. 1. The SEY coefficient δ is then calculated based on the impact kinetic energy and the incident angle. We use Vaughan's formula [33] considering the incident impact angle [34]. In addition, the suggested model in [4] is used for low impact energies. Then, an effective electron is reemitted from the impact position. Its velocity magnitude is given from a Gaussian distribution of velocities with a mean value of 4 eV and a standard deviation of 2 eV, and the launching angle is obtained using a cosine-law distribution [10].

After the mth impact, the effective-electron weighting coefficient is calculated as [35]

$$W_m^i = \prod_{k=1}^{m} \delta_k^{(i)} \tag{7}$$

where i denotes the ith effective electron, k is the index for each impact, and δ_k^i is the SEY coefficient after each impact.

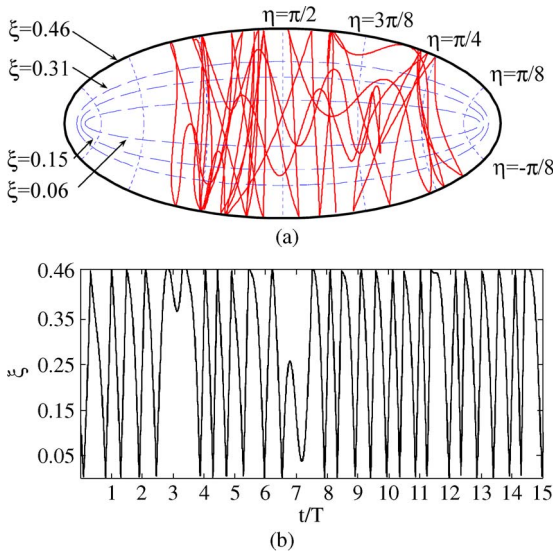

Fig. 2. (a) Electron motion in an elliptical waveguide. (b) Radius of an effective electron versus normalized time.

To predict the occurrence of a multipactor, the enhanced counter function is used [35]. This function calculates the weighted sum of the N effective electrons and divides it by the initial total number of effective electrons N, i.e.,

$$e_n/e_0 = \left(\sum_{j=1}^{N} W_n^j\right)/N. \tag{8}$$

Typically, when the value of (8) is greater than 1, a multipactor discharge has occurred [10], [35].

III. Numerical Results

A. Electron Trajectory

In Fig. 2(a), the trajectory of an effective electron with an applied electromagnetic field for the fundamental RF mode is plotted for 40 impacts. This electron has been launched from the position $\xi = 0.1186$ and $\eta = -\pi/3$ within a waveguide with $e = 0.9$ and a semiminor axis length of $b = 0.5$ mm. In addition, the applied equivalent voltage Ve is 60 V, and the working frequency is 1 GHz. Therefore, the frequency–gap product $f \times d$ is 1 ($d = 2b$).

Considering the working frequency and the waveguide dimensions, we are working below the cutoff frequency f_c suitable for iris application [24]–[26]. If the working frequency is greater than the cutoff frequency, the frequency–gap product will be greater than 78, which corresponds to very high order multipactor modes.

Note that the equivalent voltage is defined as the integral of the electric field along the vertical axis over a length $2b$, as follows:

$$\mathrm{Ve} = 2\rho \int_0^b E_\xi(\eta = \pi/2, \omega t = 0, \xi)\sqrt{U}\, d\xi. \tag{9}$$

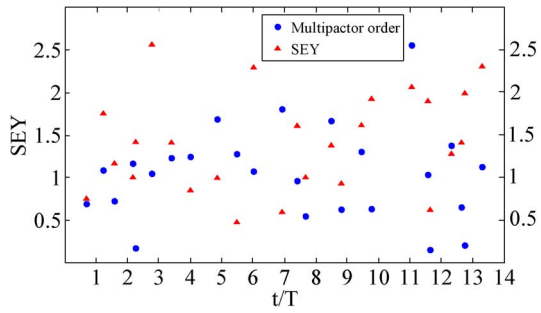

Fig. 3. SEY coefficients and multipactor orders as a function of the normalized time.

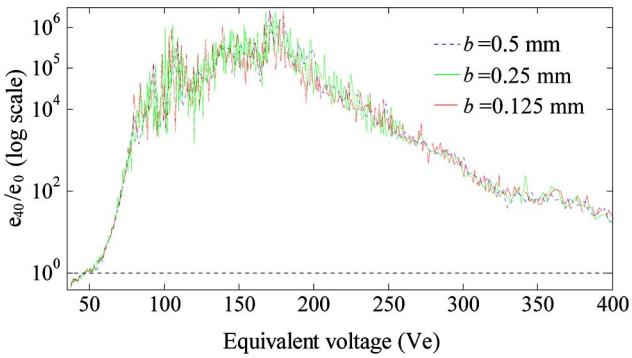

Fig. 4. Enhanced counter function as a function of the equivalent voltage for three different values of the semiminor axis length when $f \times d = 1$.

The radius of the electron trajectory [see Fig. 2(a)] as a function of the normalized time is shown in Fig. 2(b). There are generally two impacts per RF period, which is characteristic of a double-sided multipactor.

B. Multipactor Breakdown Thresholds

According to the algorithm described in Section II, we have used the enhanced counter function to predict multipactor RF breakdown thresholds. The enhanced counter function uses SEY coefficients for RF breakdown prediction. SEY coefficients and multipactor orders as a function of the normalized time for the electron tracked in Fig. 2 are shown in Fig. 3. The average SEY coefficient is greater than 1 where a multipactor can occur. The average multipactor order over 2000 RF periods is 1.03, which indicates that, to a first order, the multipactor is double sided.

The multipactor thresholds have been obtained as a function of the frequency–gap product $f \times d$. We considered 360 effective electrons in the simulation, which is a typical value to reach stable results [10], [15], [35]. Simulations using more effective electrons have been performed, concluding that a population of 360 electrons is enough to achieve the convergence region of the algorithm. There are a large set of possible f and d values for a given $f \times d$. To ensure that we have stable multipactor resonant orbits, the enhanced counter function has been calculated for three different values of $f \times d$ as a function of the equivalent voltage for $n = 40$ impacts. These curves are plotted in Fig. 4 for silver. The multipactor threshold is exceeded (enhanced counter function > 1) at an equivalent voltage of 47 V for $e = 0.9$. The material properties used for the

TABLE I
SECONDARY ELECTRON EMISSION PROPERTIES of SILVER

$E_{max}(ev)$	$\delta_{\max}$	$E_1(ev)$	$E_2(ev)$
165	2.22	30	5000

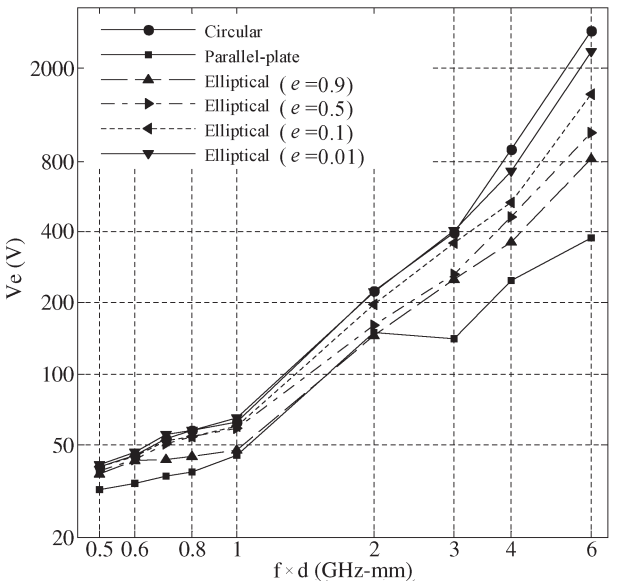

Fig. 5. Multipactor breakdown thresholds in an elliptical waveguide for four different values of eccentricity compared with multipactor breakdown thresholds in parallel-plate and circular waveguides ($f = 1$ GHz).

SEY coefficients of silver are given in Table I [4]. In this table, the primary electron impact kinetic energy that yields $\delta = \delta_{\max}$ is $E_{\max}$, and the primary electron impact kinetic energies that yield $\delta = 1$ are denoted by E_1 and E_2. As can be seen, all three curves behave similarly, demonstrating the existence of a stable first-order multipactor event.

RF breakdown thresholds were calculated for four values of the eccentricity $e = 0.01$, 0.1, 0.5, and 0.9; the results are plotted versus the frequency–gap product in Fig. 5. These results are compared with parallel-plate and circular waveguides extracted from [15]. In this figure, the diameter of the circular waveguide and the distance between the plates in the parallel-plate waveguide are d. In addition, $d = 2b$ for the elliptical waveguide, where b is the semiminor axis length. It can be seen that the thresholds increase with decreasing eccentricity. The elliptical waveguide breakdown thresholds approach those of the parallel-plate waveguide as e approaches unity. On the other hand, when e is near 0, as should be the case, the elliptical waveguide breakdown threshold approaches that of the circular waveguide. The exact differences between the circular waveguide thresholds and the elliptical waveguide ones with $e = 0.01$ are given in Table II, where significant discrepancies are not observed.

IV. CONCLUSION

Multipactor RF breakdown thresholds in an elliptical waveguide have been obtained using the effective-electron approach combined with the Monte Carlo method. The electron trajectory equations of motion were derived in elliptical coordinates using the velocity Verlet method and numerically solved using 200 time steps per RF period. The electromagnetic field of the fundamental elliptical waveguide mode TE_{c11} was applied to the motion equations. The results are compared with circular and parallel-plate waveguides as limiting cases, with good agreement. When the eccentricity of the elliptical waveguide is close to 1, the RF breakdown thresholds approach those of the parallel-plate waveguide. Similarly, when the eccentricity is close to 0, the results are close to those of the circular waveguide.

TABLE II
RF VOLTAGE THRESHOLDS (IN VOLTS) FOR AN ELLIPTICAL WAVEGUIDE WITH $e = 0.01$ AND RELATIVE ERRORS COMPARED WITH A CIRCULAR WAVEGUIDE

f.d	Elliptical waveguide (V)	Relative error (%)
0.5	41	2.5000
0.6	46	2.2222
0.7	55	3.7736
0.8	57.5	0.8772
1	65	4.8387
2	222	1.3333
3	405	1.2500
4	730	18.8889
6	2350	18.9655

REFERENCES

[1] A. J. Hatch and H. B. Williams, "Multipacting modes of high-frequency gaseous breakdown," *Phys. Rev.*, vol. 112, no. 3, pp. 681–685, Nov. 1958.
[2] R. Udiljak, D. Anderson, M. Lisak, J. Puech, and V. E. Semenov, "Multipactor in a waveguide iris," *IEEE Trans. Plasma Sci.*, vol. 35, no. 2, pp. 388–395, Apr. 2007.
[3] V. E. Semenov, E. Rakova, R. Udiljak, D. Anderson, M. Lisak, and J. Puech, "Conformal mapping analysis of multipactor breakdown in waveguide irises," *Phys. Plasmas*, vol. 15, no. 3, pp. 033501-1–033501-8, Mar. 2008.
[4] C. Vicente, M. Mattes, D. Wolk, B. Mottet, H. L. Hartnagel, J. R. Mosig, and D. Raboso, "Multipactor breakdown prediction in rectangular waveguide based components," in *Proc. IEEE MTT-S Int. Microw. Symp. Dig.*, Jun. 2005, pp. 1055–1058.
[5] A. G. Sazontov, V. A. Sazontov, and N. K. Vdovicheva, "Multipactor breakdown prediction in a rectangular waveguide: Statistical theory and simulation results," *Contrib. Plasma Phys.*, vol. 48, no. 4, pp. 331–346, May 2008.
[6] V. E. Semenov, E. I. Rakova, D. Anderson, M. Lisak, and J. Puech, "Multipactor in rectangular waveguides," *Phys. Plasmas*, vol. 14, no. 3, pp. 033501-1–033501-8, Mar. 2007.
[7] I. A. Kossyi, G. S. Lukyanchikov, V. E. Semenov, E. I. Rakova, D. Anderson, M. Lisak, and J. Puech, "Polyphase (non-resonant) multipactor in rectangular waveguides," *J. Phys. D, Appl. Phys.*, vol. 41, no. 6, pp. 065203-1–065203-8, Mar. 2008.
[8] A. Dexter and R. Seviou, "Rapid generation of multipactor charts by numerical solution of the phase equation," *J. Appl. Phys.*, vol. 38, no. 9, pp. 1383–1389, Apr. 2005.
[9] R. L. Geng, P. Goudket, R. G. Carter, S. Belomestnykh, H. Padamsee, and D. M. Dykes, "Dynamical aspects of multipacting induced discharge in a rectangular waveguide," *Nucl. Instrum. Methods Phys. Res. A, Accel. Spectrom. Detect. Assoc. Equip.*, vol. 538, no. 1–3, pp. 189–205, Feb. 2005.
[10] A. M. Pérez, C. Tienda, C. Vicente, S. Anza, J. Gil, B. Gimeno, V. E. Boria, and D. Raboso, "Prediction of multipactor breakdown thresholds in coaxial transmission lines for traveling, standing, and mixed waves," *IEEE Trans. Plasma Sci.*, vol. 37, no. 10, pp. 2031–2040, Oct. 2009.
[11] I. A. Kossyi, G. S. Luk'yanchikov, V. E. Semenov, N. A. Zharova, D. Anderson, M. Lisak, and J. Puech, "Experimental and numerical investigation of multipactor discharges in a coaxial waveguide," *J. Phys. D, Appl. Phys.*, vol. 43, no. 34, pp. 345206-1–345206-8, Aug. 2010.

[12] D. Anderson, M. Lisak, V. E. Semenov, J. Puech, and R. Udiljak, "Multipactor in a coaxial transmission line. I. Analytical study," *Phys. Plasmas*, vol. 14, no. 3, pp. 033508-1–033508-11, Mar. 2007.
[13] E. Semenov, N. Zharova, R. Udiljak, D. Anderson, M. Lisak, and J. Puech, "Multipactor in a coaxial transmission line. II. Particle-in-cell simulations," *Phys. Plasmas*, vol. 14, no. 3, pp. 033509-1–033509-7, Mar. 2007.
[14] T. Abe, T. Kageyama, K. Akai, K. Ebihara, H. Sakai, and Y. Takeuchi, "Multipactoring zone map of an RF input coupler and its application to high beam current storage rings," *Phys. Rev. ST Accel. Beams*, vol. 9, no. 6, pp. 062002-1–062002-8, Jun. 2006.
[15] M. Pérez, V. E. Boria, B. Gimeno, S. Anza, C. Vicente, and J. Gil, "Multipactor analysis in circular waveguides," *J. Electromagn. Waves Appl.*, vol. 23, no. 11, pp. 1575–1583, Sep. 2009.
[16] V. Semenov, E. Rakova, N. Zharova, D. Anderson, M. Lisak, and J. Puech, "Simulations of the multipactor effect in hollow waveguides with wedge-shaped cross section," *IEEE Trans. Plasma Sci.*, vol. 36, no. 2, pp. 488–493, Apr. 2008.
[17] V. E. Semenov, E. I. Rakova, A. G. Sazontov, I. M. Nefedov, V. I. Pozdnyakova, I. A. Shereshevskii, D. Anderson, M. Lisak, and J. Puech, "Simulations of multipactor thresholds in shielded microstrip lines," *J. Phys. D, Appl. Phys.*, vol. 42, no. 20, p. 205204, Sep. 2009.
[18] Á. Coves, G. Torregrosa-Penalva, C. Vicente, B. Gimeno, and V. E. Boria, "Multipactor discharges in parallel-plate dielectric-loaded waveguides including space-charge effects," *IEEE Trans. Electron Devices*, vol. 55, no. 9, pp. 2505–2511, Sep. 2008.
[19] M. Jiménez, B. Gimeno, C. Miquel-Espanya, D. Raboso, S. Anza, C. Vicente, J. Gil, F. Quesada, A. Álvarez, M. Taroncher, M. Reglero, and V. E. Boria, "Analysis of the electromagnetic radiation generated by a multipactor discharge occurring within a microwave passive component," *J. Phys. D, Appl. Phys.*, vol. 43, no. 39, pp. 395501-1–395501-7, Sep. 2010.
[20] M. Mostajeran and M. Lamehi Rachti, "On the phase stability in two-sided multipactor," *Nucl. Instrum. Methods Phys. Res. A, Accel. Spectrom. Detect. Assoc. Equip.*, vol. 615, no. 1, pp. 1–5, Mar. 2010.
[21] S. Anza, C. Vicente, J. Gil, V. E. Boria, B. Gimeno, and D. Raboso, "Nonstationary statistical theory for multipactor," *Phys. Plasmas*, vol. 17, no. 6, pp. 062110-1–062110-11, Jun. 2010.
[22] W. Cui, Z. Wang, T. Jiang, D. Wang, W. Ma, and L. Ran, "The prevention of multipactor discharge in rectangular waveguide loaded with uniaxial metamaterial," in *Proc. PIERS*, Hangzhou, China, 2008, pp. 760–764.
[23] L. Accatino, G. Bertin, and M. Mongiardo, "Elliptical cavity resonators for dual-mode narrow-band filters," *IEEE Trans. Microw. Theory Tech.*, vol. 45, no. 12, pp. 2393–2401, Dec. 1997.
[24] V. E. Boria and B. Gimeno, "Waveguide filters for satellites," *IEEE Microw. Mag.*, vol. 8, no. 5, pp. 60–70, Oct. 2007.
[25] B. Gimeno and M. Guglielmi, "Full wave network representation for rectangular, circular, and elliptical to elliptical waveguide junctions," *IEEE Trans. Microw. Theory Tech.*, vol. 45, no. 3, pp. 376–384, Mar. 1997.
[26] J. Xu, W. Wang, L. Lye, Y. Wei, and Y. Gong, "Study of corrugated elliptical waveguides for slow-wave structures," *IEEE Trans. Electron Devices*, vol. 54, no. 1, pp. 151–156, Jan. 2007.
[27] S. Marini, A. Coves, V. E. Boria, and B. Gimeno, "Full-wave modal analysis of slow-wave periodic structures loaded with elliptical waveguide," *IEEE Trans. Electron Devices*, vol. 57, no. 2, pp. 516–524, Feb. 2010.
[28] D. A. Goldberg, L. J. Laslett, and R. A. Rimmer, "Modes of elliptical waveguides: A correction," *IEEE Trans. Microw. Theory Tech.*, vol. 38, no. 11, pp. 1603–1608, Nov. 1990.
[29] G. D. Tsogkas, J. A. Roumeliotis, and S. P. Savaidis, "Cutoff wavelengths of elliptical metallic waveguides," *IEEE Trans. Microw. Theory Tech.*, vol. 57, no. 10, pp. 2406–2415, Oct. 2009.
[30] S. J. Zhang and Y. Shen, "Eigenmode sequence for an elliptical waveguide with arbitrary ellipticity," *IEEE Trans. Microw. Theory Tech.*, vol. 43, no. 1, pp. 227–230, Jan. 1995.
[31] G. Blanch, *Handbook of Mathematical Function*, M. Abramowitz and I. A. Stegun, Eds. New York: Dover, 1972, p. 721.
[32] Q. Spriter and M. Walter, "Classical molecular dynamics simulation with the Velocity Verlet algorithm at strong external magnetic fields," *J. Comput. Phys.*, vol. 152, no. 1, pp. 102–119, Jun. 1999.
[33] J. R. M. Vaughan, "A new formula for secondary emission yield," *IEEE Trans. Electron Devices*, vol. 36, no. 9, pp. 1963–1967, Sep. 1989.
[34] A. Shih and C. Hor, "Secondary emission properties as a function of the electron incidence angle," *IEEE Trans. Electron Devices*, vol. 40, no. 4, pp. 824–829, Apr. 1993.
[35] E. Somersalo, P. Ylä-Oijala, D. Proch, and J. Sarvas, "Computational methods for analyzing electron multipacting in RF structures," *Part. Accel.*, vol. 59, pp. 107–141, 1998.

Ali Frotanpour (S'10) was born in Tehran, Iran, on September 17, 1985. He received the A.D. degree in electronics from the Islamic Republic of Iran Broadcasting University, Tehran, Iran, in 2006 and the B.Sc. degree in communication engineering from Khayyam University, Mashhad, Iran, in 2008. He is currently working toward the M.Sc. degree in electrical engineering at Shahed University, Tehran, Iran.

Since July 2009, he has been collaborating with the satellite communications group of Iran Telecommunication Research Center on traveling-wave tube-amplifier predistortion linearizers, dual-mode waveguide filters, and multipactor effect. His research interests include the analysis of multipactor radio-frequency breakdown, printed antennas with linear and circular polarization, and microwave filters.

Gholamreza Dadashzadeh (M'05) was born in Urmia, Iran, in 1964. He received the B.Sc. degree in communication engineering from Shiraz University, Shiraz, Iran, in 1992 and M.Sc. and Ph.D. degrees in communication engineering from Tarbiat Modarres University, Tehran, Iran, in 1996 and 2002, respectively.

From 1998 to 2003, he has worked as the Head Researcher of the Smart Antenna for Mobile Communication Systems and the wireless local-area network 802.11 project with the radio communications group of Iran Telecommunication Research Center (ITRC). From 2004 to 2008, he was the Dean of the Communications Technology Institute, ITRC. He is currently an Assistant Professor with the Department of Electrical Engineering, Shahed University, Tehran. He has published more than 70 papers in referred journals and international conferences in the area of antenna design and smart antennas.

Dr. Dadashzadeh is a member of the Institute of Electronics, Information, and Communication Engineers of Japan and the Iranian Association of Electrical and Electronics Engineers. He received the first degree of national researcher in 2007 from Iran's Ministry of Information and Communications Technology.

Mahmoud Shahabadi received the B.Sc. and M.Sc. degrees from the University of Tehran, Tehran, Iran, and the Ph.D. degree from Technische Universitaet Hamburg-Harburg, Germany, in 1988, 1991, and 1998, respectively, all in electrical engineering.

Since 1998, he has been an Assistant Professor and then an Associate Professor with the School of Electrical and Computer Engineering, University of Tehran. From 2001 to 2004, he was a Visiting Professor with the Department of Electrical and Computer Engineering, University of Waterloo, Canada. Additionally, he is a Cofounder and Chief Technical Officer of MASSolutions Inc., which is a Waterloo-based company with a focus on advanced low-profile antenna array systems. His research interests and activities encompass various areas of microwave and millimeter-wave engineering, as well as photonics. Computational electromagnetics for microwave engineering and photonics are his special interest. He is currently conducting research and industrial projects in the field of antenna engineering, terahertz engineering, photonic crystals, plasmonics, left-handed materials, and holography.

Dr. Shahabadi was the recipient of the 1998/1999 Prize of the German Metal and Electrical Industries, Nordmetall, for his contribution to the field of millimeterwave holography and spatial power combining.

Benito Gimeno (M'01) was born in Valencia, Spain, on January 29, 1964. He received the Licenciado degree in physics and the Ph.D. degree from the Universidad de Valencia, Valencia, Spain, in 1987 and 1992, respectively.

From 1987 to 1990, he was a Fellow with the Universidad de Valencia. Since 1990, he has been an Assistant Professor with the Departamento de Fca Aplicada y Electromagnetismo and the Instituto de Ciencia de Materiales, Universidad de Valencia, where he became an Associate Professor in 1997 and a Full Professor in 2010. In 1994 and 1995, he was a Research Fellow with the European Space Research and Technology Centre of the European Space Agency. In 2003, he obtained a Fellowship from the Spanish Government for a short stay at the Universita degli Studi di Pavia, Italy, as a Visiting Scientific. His current research interests include the areas of computer-aided techniques for the analysis of microwave and millimeter-wave passive components for space applications, waveguides, and cavity structures including dielectric objects, electromagnetic band-gap structures, frequency selective surfaces, and nonlinear phenomena appearing in power microwave subsystems and particle accelerators (multipactor effect, corona effect, and passive intermodulation phenomena).